Ocean Dynamics (2024) 74:525–537
https://doi.org/10.1007/s10236-024-01617-8

# Experimental and numerical investigation of shelf flow crossing over a strait

**Joseph Kuehl**[1] · **Vitalii A. Sheremet**[2]

Received: 23 October 2023 / Accepted: 25 April 2024 / Published online: 20 May 2024


**Abstract**
Motivated by the phenomenon of Scotian Shelf Crossover events, the problem of a shelf flow that is interrupted by a strait is considered. Laboratory experiments in a rotating tank with barotropic and baroclinic flow over flat and sloping shelves confirm that the flow is steered by the bathymetric contours and mainly circumnavigates the gulf. In order to jump across the strait, as suggested by earlier theories, the flow must have unrealistically high Rossby numbers. However, the near bottom friction relaxes the bathymetric constraint and causes the formation of a peculiar jet crossing the strait diagonally. For the dissipation values such that a half of the transport goes around the gulf and half crosses the strait diagonally, the diagonal crossover jet becomes most evident. Numerical solutions for realistic values of the frictional parameter reproduce the results of the laboratory experiments and consideration of the actual Gulf of Maine bathymetry reproduces patterns similar to those observed by drift trajectories and in the satellite derived sea surface temperature fields.

**Keywords** Geophysical fluid dynamics · Topographic control · Shelf flow

## 1 Introduction

This work is motivated by the phenomenon of Scotian Shelf Crossover events. Cold and fresh Scotian Shelf Water (SSW) normally enters the Gulf of Maine around Cape Sable and Browns Bank (Smith 1983b) following along the isobaths (see Fig. 1, dashed line). It takes the plume about 6-8 months to circumnavigate the Gulf, before reaching Georges Bank (Mountain and Manning 1994; Manning et al. 2009). However, intermittently some water mass flows directly from the Scotian Shelf to Georges Bank (Bisagni and Smith 1998) over the Northeast Channel (NEC), a phenomenon known as the SSW "crossover" events. These events are most dramatic (visible) in spring when the contrast in water properties between SSW on Browns Bank and Georges Bank water on the Northeast Peak is largest, due to the arrival of a freshwater pulse from the Gulf of St. Lawrence (Smith 1983a, 1989; Smith et al. 1997). The spring is also the time when the stratification is weaker, and the bathymetric steering is therefore more important. The SSW crossovers, rich in plankton, have important implications for Georges Bank biological productivity (Wishner et al. 2003).

The primary driving mechanism(s) for SSW crossovers are elusive. Obvious candidates include (a) increased inertia of the along-shelf flow in the shelf/slope front lying over the upper slope, (b) instability of the SSW front around Browns Bank, (c) synoptic wind events, (d) time dependent forcing such as tide, and (e) warm-core rings from the Gulf Stream. The along-shelf flux of fresh water over the western Scotian Shelf peaks in late winter/early spring, and forms a SSW front around the southwestern flank of Browns Bank. Moored measurements show that the axial (inflow) current component in NEC reaches a maximum during this period, and the near-surface cross-channel component tends to veer toward Georges Bank during February - March, consistent with crossover (Smith et al. 1997). In March of 1997 multiple

Responsible Editor: Pierre F.J. Lermusiaux

Vitalii A. Sheremet contributed equally to this work

✉ Joseph Kuehl
jkuehl@udel.edu

Vitalii A. Sheremet
vsheremet@whoi.edu

[1] Department of Mechanical Engineering, University of Delaware, 130 Academy Street, Newark, Delaware 19716, USA

[2] Department of Physical Oceanography, Woods Hole Oceanographic Institution, MS#21, Woods Hole, Massachusetts 02543, USA

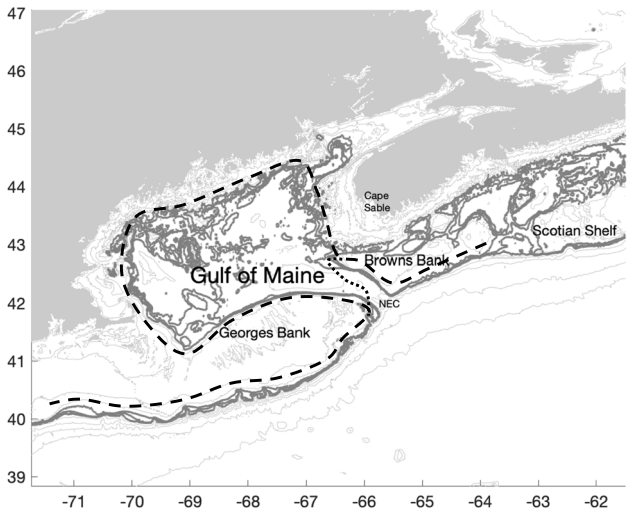


**Fig. 1** Topographic map of the Gulf of Maine. The 125, 150 and 175m isobaths are highlighted and two circulation patterns are indicated by the dashed and dotted thick black lines. A similar map with upper and lower layer circulation patterns during the summer stratified season can be found in Beardsley et al. (1997)

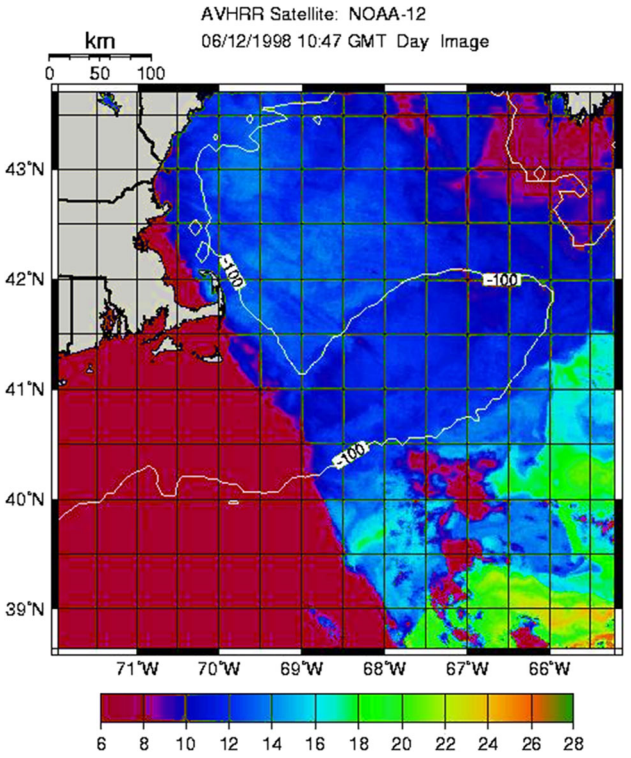


**Fig. 2** SST image of the Northeast Channel showing flow into and around Gulf of Maine. No crossover is observed. Color bar is in degrees C. The magenta patch in the lower left is due to clouds and satellite communication gaps

SeaSoar sections were conducted across SSW plume revealing its internal structure and the relationship to the shelfbreak front (Lee and Brink 2000). During winter/spring of 1999, a period of deployment of moorings in the NEC, several crossover events were documented (Smith et al. 2003). While attempts to link interannual variability in along-shelf fresh water flux with observed crossover events have been unsuccessful to date (Bisagni et al. 1996), it is conceivable that the SSW front is locally unstable during winter and may form eddy features which carry SSW directly to Georges Bank. We note that many satellite derived sea surface temperature (SST) fields exhibit a peculiar feature: the crossover plume does not always originate from the corner of Browns Bank but rather crosses the channel diagonally, north-south (Figs. 2, 3 and 4; Fig. 2 shows no crossover, Fig. 3 shows a diagonal crossover, and Fig. 4 shows a more direct crossover). Especially good examples may be found in Smith et al. (2003), (Fig. 12cg). In addition to the SST fields, such crossover events are also present in the 1995-1999 GLOBEC drifter data (Limeburner 2019). In Fig. 5, all GLOBEC drifters which crossover the NEC channel are shown. Notice that several of the drifters exhibit tracks consistent with the peculiar diagonal crossover. While these drifter tracks and SST images do not prove the existence of diagonal crossover, they do serve as sufficient motivation for the current study. The goal of which is to isolate the steady state dynamics of barotropic and baroclinic shelf flow interrupted by a strait.

Considering the dynamical complexity of the SSW crossovers and shelf/slope frontal system, several model studies have been undertaken to isolate potentially important processes which may produce SSW crossovers. Klinger (1994); Garret (1995); Williams et al. (2001) studied the conditions for inviscid separation of the flow from a cape, and showed that a barotropic shelf-break current must flow smoothly around a sharp bend (like the southwest tip of Browns Bank) for realistic parameters (small Rossby numbers), suggesting that other factors must play a role in the crossover. Cho et al. (2002) showed numerically that sufficiently strong density stratification is capable of overcoming the depth variation constraints and promote flow across the channel. Sheremet (2001) suggested that multiple steady flow patterns are possible in such flow systems (barotropic cases Sheremet and Kuehl 2007; Kuehl and Sheremet 2009 baroclinic case Kuehl and Sheremet 2014). Chapman (2003) studied numerically a separation of an advectively trapped buoyancy current at a bathymetric bend and simulated two different flow patterns caused by the flow inertia. Wolfe and Cenedese (2006) conducted laboratory experiments with a buoyant coastal current flowing over variable bathymetry and studied the associated eddy generation.

The studies referenced above are very relevant for explaining the local effects of the cape corner or a bathymetric gap on

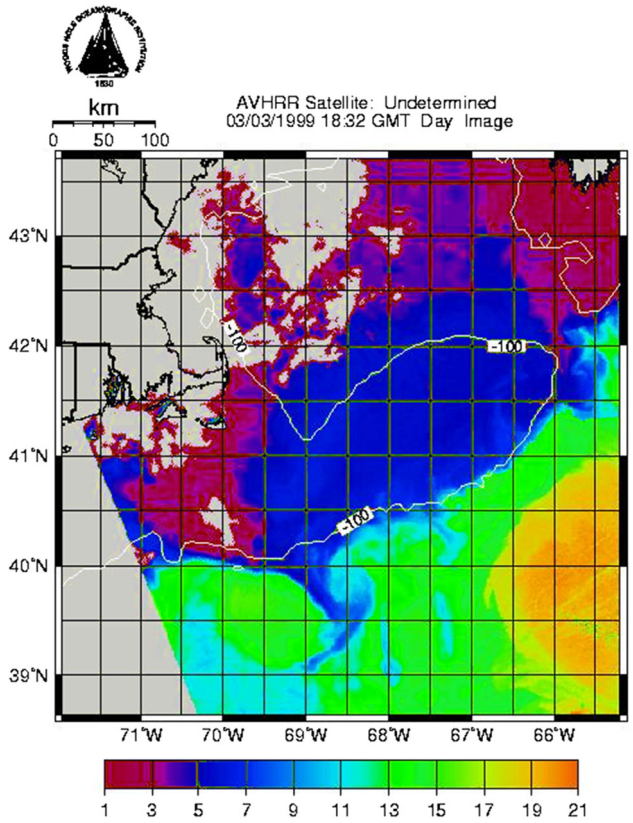


**Fig. 3** SST image of the Northeast Channel showing the peculiar diagonal crossover pattern. Color bar is in degrees C. The gray color areas are due to clouds and satellite communication gaps

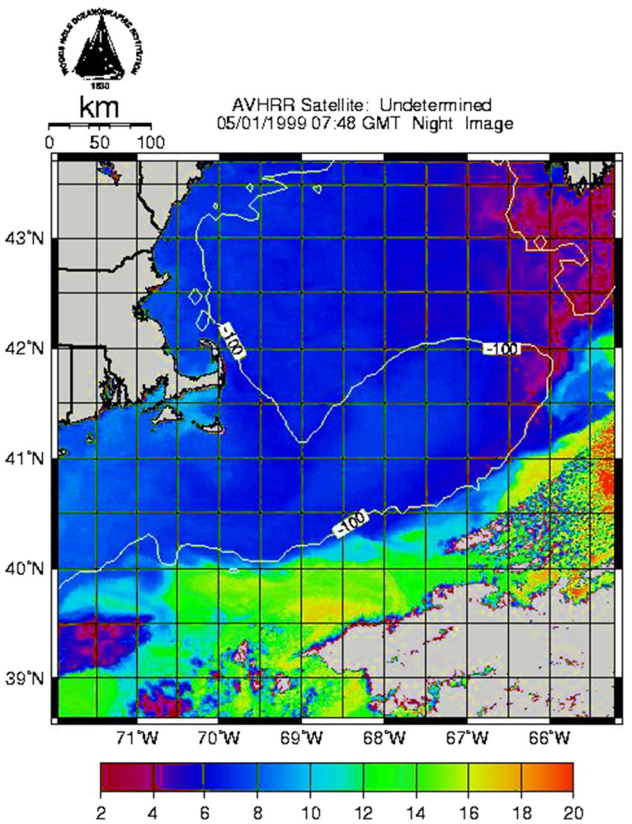


**Fig. 4** SST image of the Northeast Channel showing a strong crossover pattern. Color bar is in degrees C. The gray color areas are due to clouds

the flow; they, however, do not capture the large scale character of the Scotian Shelf, Gulf of Maine and Georges Bank as a whole dynamical system. Despite the range of dynamical complexity and various consideration (a-e listed above) that may influence SSW crossover events, this manuscript presents a subtle mechanism in which no such complexity is required. Indeed, only the splitting of a geostrophic contour ($f/H$, the Coriolis parameter divided by depth) in the NEC, with one branch circumnavigating the Gulf of Maine and the other branch going directly to Georges Bank where they reconnect, is required to produce the peculiar diagonal flow patterns across the NEC. In Section 2, we introduce a simplified source-sink driven laboratory model of the shelf flow representing the essential geometry. In Section 3, we demonstrate that while the inertia indeed promotes the crossovers, the flow across the channel is present even in the linear case due to the bottom drag. Furthermore, such flow has a very peculiar diagonal pattern which is conspicuous in many satellite derived surface temperature fields. In Section 4, we define a numerical representation of the general case of a shelf flow crossing a strait. In Section 5, we reproduce the same pattern numerically using realistic parameters and also apply our

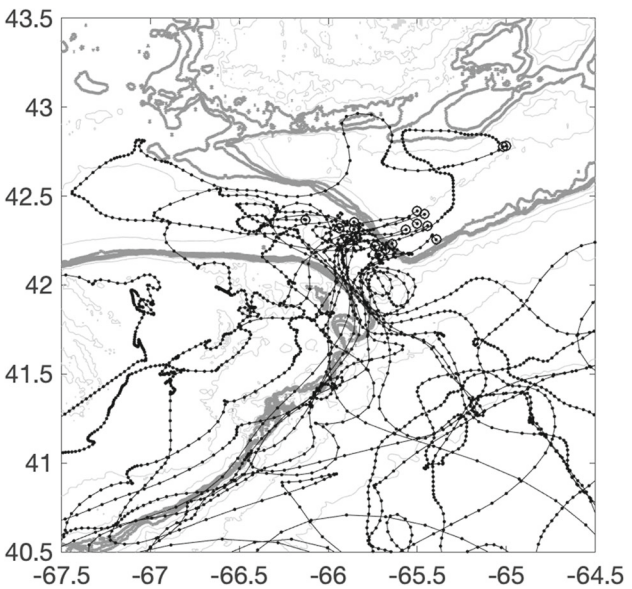


**Fig. 5** GLOBEC drifter tracks showing NEC crossover events between 1995-1999, superimposed on NEC topography. The 125, 150 and 175m isobaths are highlighted and drifter tracks are shown as dotted lines with open circles indicating deployment location

numerical model to the actual Gulf of Maine bathymetry. And finally, we offer conclusions in Section 6.

## 2 Experimental setup

To model the basic dynamics of the NEC, we consider the 2m-diameter, rotating, cylindrical tank depicted in Fig. 6. Into the tank, a 1.2m-diameter, 0.3m-tall cylindrical insert was placed. On to the cylindrical insert, a 2cm tall flat ring was placed with an inner radius of 0.4m and outer radius of 0.6m. A second, identical ring is placed on top of the first. Out of the top ring, a 0.2m (along its center arc) gap was cut. Onto the upper loop, a sloping ridge was inserted with a 2.5cm peak at the center, which provides a linear sloping shelf topography from the center peak to the edges of the ridge. Finally, a vertical ridge was inserted into the center of the top ring that extends to within 0.1m of the gap edge. The tank was filled with fresh water to a level such that the depth at the shelfbreak was approximately 2.5cm: in the sloping shelf case, the topography was rounded and smoothed as it turns the corners and the depth near the ridges was vanishing while in the flat shelf case the depth over the shelf was nearly uniform at 2.5cm. The tank was rotated in the range 0.1-0.5 rad/s. Table 1 contains a list of the relevant parameters for the oceanographic, laboratory and numerical cases. Note, we have chosen to define the Rossby number, $R_0$, based on the bulk flow properties that are experimentally accessible. The oceanic Rossby number characteristic of a shelfbreak jet would be higher.

The sloping ridges represent the Scotian Shelf and Georges Bank, the gap represents the NEC and the depression over the center of the insert represents the Gulf of Maine. Opposite the NEC, a vertical ridge was inserted to separate the Georges Bank and Scotian shelf sides of the ridge. The system is forced at these points. The generated flow propagates along the Scotian Shelf (following the isobaths) until it encounters the NEC. For weak forcing, potential vorticity constraints are sufficient to restrict the flow to the sloping shelf which then traverses the Gulf of Maine and circles Georges Bank before reaching the sink. For larger forcing amplitudes, vorticity constraints are not sufficient to constrain the flow to the sloping shelf and it must negotiate the NEC. The flow was visualized with neutrally buoyant dye injection, which was introduced with a thin needle at the layer middle depth. One dye streak was injected directly at the shelf break edge and the other was injected in the middle of the shelf, both upstream of the NEC on Browns Bank.

## 3 Experimental results

The objective of this experimental investigation was to reproduce and analyze the peculiar cross-over flow pattern shown in Figs. 2, 3 and 4. It is observed that during such cross-over events, SSW collects on the Gulf of Maine side of Browns Bank before transiting diagonally across the NEC and encountering the outer (Atlantic ocean) corner of Georges Bank.

### 3.1 Experiment 1

The first set of experiments was conducted without the sloping shelf insert. Dye visualization was used to track the flow pattern as a function of table rotation rate $f = 2\Omega$ and flow rate $Q$. The water depth over the flat shelf was set to $2.5\,cm$ and rotation rate was set to $f = 0.2s^{-1}$. The tank was filled with fresh water and rotated. The tank was allowed to reach solid body rotation before the pumping was initiated. Pumping rates of $Q = 31,\ 43,\ 62\,cm^3/s$ were considered and the resulting flow patterns can be seen in Fig. 7. Note that when

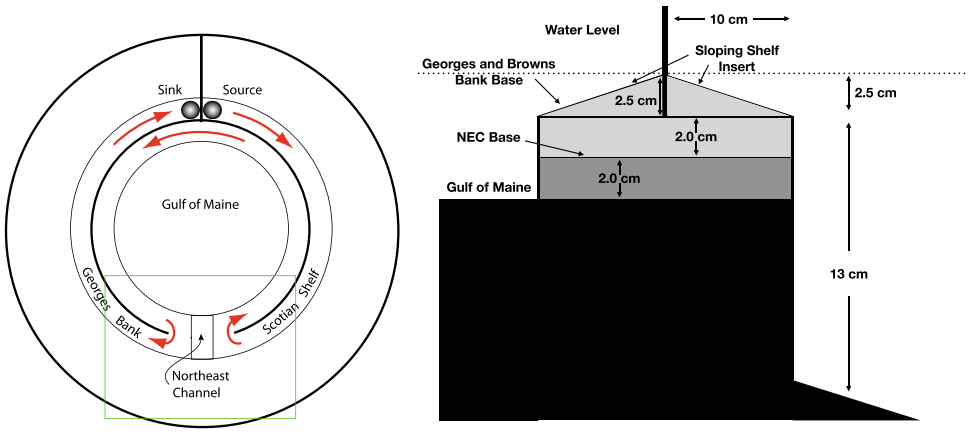


**Fig. 6** Experimental setup. Left) Top down view. Right) Cross-section view radially through the NEC. Dotted line represent water level, light grey triangle represents sloping shelf insert, light grey rectangle represents upper ring insert, dark grey represents lower ring insert and black represents cylindrical insert

**Table 1** Comparison of key parameters and representative values between the ocean, laboratory and numerical model

| Parameters | Ocean | Laboratory experiment | Numerical model |
|---|---|---|---|
| Shelf width, $L_*$ | 100km | 10cm | 1, Horizontal (x,y) scale |
| Shelfbreak depth, $H_*$ | 100m | 2.5cm | 1, Vertical z scale |
| Coriolis parameter, $f$ | $2\Omega \sin\varphi = 10^{-4}s^{-1}$ | $2\Omega = 0.5s^{-1}$ | 1/(Time scale) |
| Shelf transport, $Q$ | 0.5 Sv | up to 62 $cm^3/s$ | 1, Stream function scale |
| Horizontal velocity, $U = Q/(H_*L_*)$ | 5 cm/s | 2.5 cm/s | O(1) |
| Rossby number, $L_*$ | 0.005 | 1.26 – 0.24 | 0 |
| Bottom drag, $R = h_E/H$ | 0.03 | 0.08 | 0.04 |

presenting the laboratory and numerical results, the images will be flipped from the traditional North up convention. In this way the inflow is from the left with positive velocity.

The topographic steps between the shelf and NEC, shelf and Gulf of Maine or NEC and Gulf of Maine can be thought of as vorticity barriers which the flow must negotiate. For the inviscid case with weak flow rates, the inertia of the current is unable to overcome this vorticity barrier and the flow is confined to the shelf region, following a path along the shelf, around the Gulf of Maine and ultimately around Georges Bank. Essentially, the flow follows geostrophic contours in a rapidly rotating fluid. At high flow rates, the inertia of the current is able to overcome the vorticity barrier and the current is able to traverse the NEC leaping directly from Browns Bank to Georges Bank. For $Q = 62\,cm^3/s$ and $43\,cm^3/s$, such leaping is observed with the larger flow rate resulting in a more direct trajectory across the NEC (both strong crossover patterns similar to Fig. 4) and the lower exhibiting a larger deflection during the transit from Browns to Georges Bank. At $Q = 31\,cm^3/s$, the inertia of the current is low enough that it can no longer break the topographic constraint, and the flow tends to be confined to the shelf region. However the outer-most fluid at the shelf edge is observed to follow a path very similar to that observed in SST image of the NEC (peculiar crossover pattern similar to Fig. 3).

As expected, a similar flow pattern trend is observed when the flow rate is held constant and the table rotation rate is varied. Figure 8 shows the results for $Q = 62\,cm^3/s$ and $f$ varying from $0.2 - 0.5s^{-1}$. For larger rotation rates, the gap presents a larger vorticity barrier than for lower rotation rates. The flow is able to overcome the vorticity barrier presented by the NEC for $f = 0.2s^{-1}$ (both strong crossover patterns similar to Fig. 4) and $0.3s^{-1}$, but assumes a similar pattern to that observed in SST images of the NEC for rotation rates of $f = 0.4s^{-1}$ and $0.5s^{-1}$ (peculiar crossover pattern similar to Fig. 3).

### 3.2 Experiment 2

To more closely represent the dynamics of the Scotian shelf, a linear sloping shelf topography was inserted onto the ridge (as described above). The table rotation rate was set to

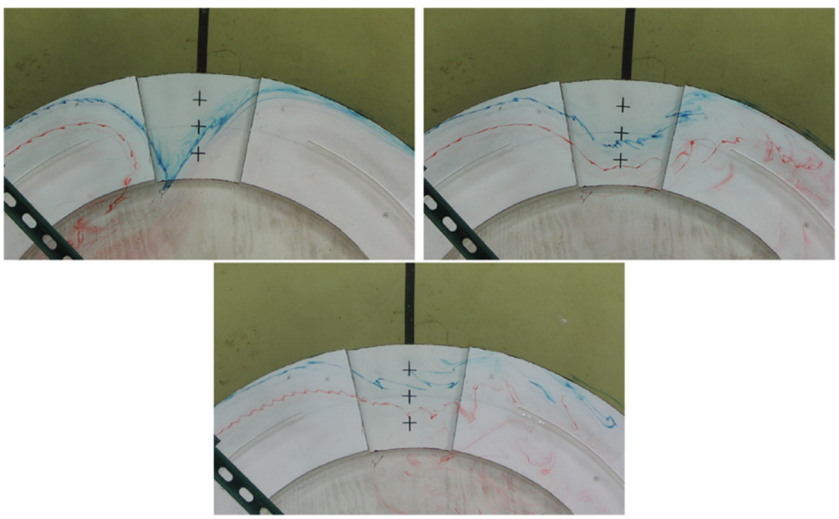

**Fig. 7** Barotropic flow pattern dependence on current transport magnitude. $f = 0.2s^{-1}$ with flow rate varying from: Upper Left) $Q = 31\,cm^3/s$, $R_o = 0.62$; Upper Right) $Q = 43\,cm^3/s$, $R_o = 0.84$; Lower) $Q = 62\,cm^3/s$, $R_o = 1.26$

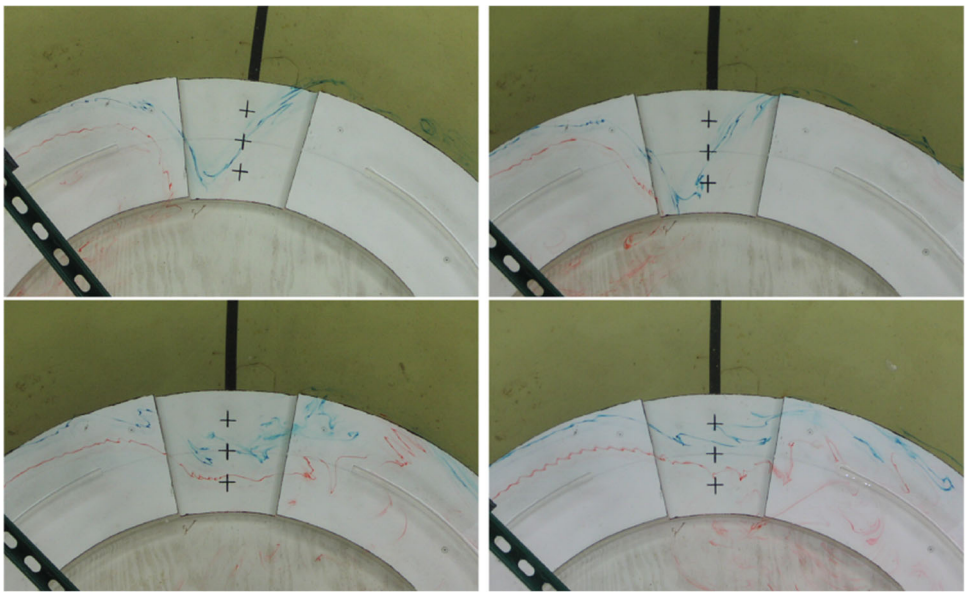

**Fig. 8** Barotropic flow pattern dependence on table rotation rate. $Q = 62\,cm^3/s$ with rotation rate varying from: Upper Left) $f = 0.5s^{-1}$, $R_o = 0.5$; Upper Right) $f = 0.4s^{-1}$, $R_o = 0.63$; Lower Left) $f = 0.3s^{-1}$, $R_o = 0.84$; Lower Right) $f = 0.2s^{-1}$, $R_o = 1.26$

$f = 0.5s^{-1}$ and flow rates of $Q = 31\,cm^3/s$ and $62\,cm^3/s$ are shown in Fig. 9. Notice that the presence of a sloping shelf topography has not significantly altered the trends previously discussed. For the lower flow rate, fluid on the interior of the shelf is confined to flow along geostrophic contours and circles the Gulf of Maine along the shelf. Fluid at the outer-most edge of the shelf is observed to follow a path very similar to that observed in SST images of the NEC (peculiar crossover pattern similar to Fig. 3). As the flow rate is increased, this flow pattern is maintained, but more of the shelf water is able to cross the geostrophic contours imposed by the sloping shelf topography and cross the NEC.

### 3.3 Experiment 3

The signal seen in the SST observations resulted from a cold, fresh plume of Scotian shelf water propagating southward. To consider the effect of such stratification on the previously discussed flow patterns, a stratified experiment was conducted. The tank was filled with seawater (from the Nantucket Sound), and the shelf flow was driven with slightly diluted seawater (with ratio 10:1 ). The density difference between layers was $\Delta\rho = 2.2 \times 10^{-3}\ g/cm^3$ with a reduced gravity $g' = g\Delta\rho/\rho = 2.2cm/s^2$. This resulted in a baroclinic Rossby radius of deformation of $L_R = \sqrt{g'H_*}/f = 4.7cm$ which is about half of shelf width, $L_* = 10cm$, and a quarter of the channel width in the laboratory. The density across the shelf break front varies seasonally, $(0.5-1.5)\times 10^{-3} g/cm^3$, therefore the internal Rossby radius of deformation is about $10km$ which is about a quarter of the NEC width. Once the lower density shelf water circulation was allowed time to setup, red dye was injected. Figure 10 shows the propagation of the lower density water along the shelf. Notice that much of the shelf water is constrained by the geostrophic contours to flow into and around the Gulf of Maine, along the shelf. However, the fluid near the outer-most edge of the shelf once again is observed to follow a path very similar to that observed in SST images of the NEC (peculiar crossover patterns similar to Fig. 3).

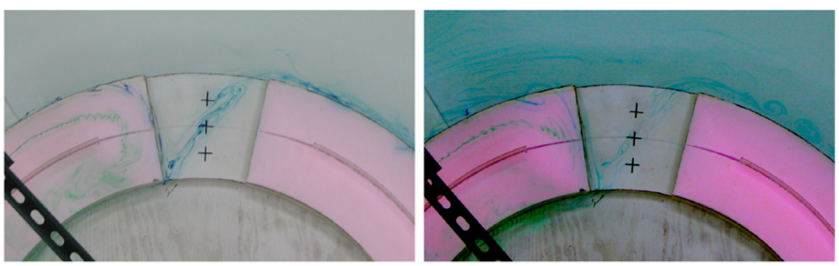

**Fig. 9** Barotropic flow pattern dependence on current transport magnitude with sloping shelf topography. $f = 0.5s^{-1}$ with flow rate varying from: Left) $Q = 31\,cm^3/s$ , $R_o = 0.24$; Right) $Q = 62\,cm^3/s$, $R_o = 0.5$

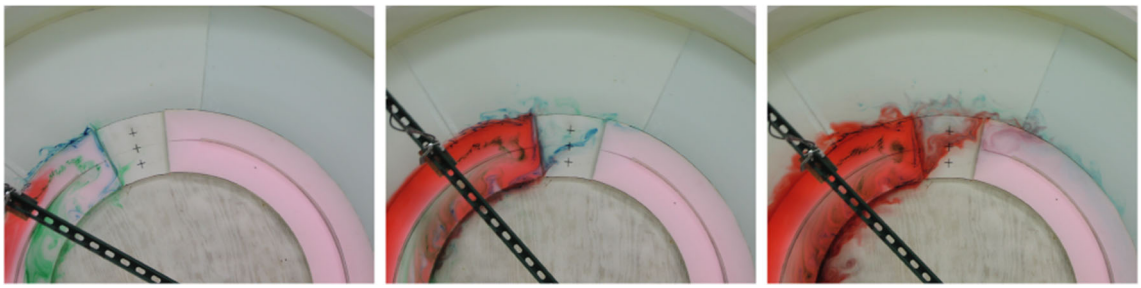

**Fig. 10** Baroclinic flow pattern progression with $f = 0.5s^{-1}$, $Q = 31cm^{3/s}$, and $R_o = 0.24$

## 4 Numerical model

The formulation of flow dynamics on the continental shelf is well known. The reader can find a good introduction in Gill (1982 Ch 10.12 on Continental Shelf Waves) and follow the references given therein. We also note that it is elucidating to consider a steady flow as a limit of a long period wave. Therefore, we start with the evolution of barotropic potential vorticity $q = (f+\zeta)/H$ equation (including the near-bottom vorticity dissipation) which captures the most robust flow features

$$\zeta_t + J(\psi, \frac{f+\zeta}{H}) = -\frac{1}{2} f \frac{h_E}{H} \zeta \tag{1}$$

coupled with an elliptic equation for the stream function $\psi(x, y, t)$

$$\nabla(\frac{1}{H}\nabla\psi) = \zeta, \tag{2}$$

where $\zeta(x, y, t)$ is the relative vorticity, $x$, $y$ horizontal coordinates, $t$ is time, $J$ is the jacobian operator, $H(x, y)$ is the fluid depth. In the oceanic case the Coriolis parameter $f = 2\Omega \sin(\varphi)$ slightly varies with latitude $\varphi$, and $\Omega$ is the earth rotation rate. In the laboratory $f = 2\Omega$ is fixed and $\Omega$ is the rotation rate of the turntable. Only the bottom friction is considered, which is characterized by the bottom boundary layer of Ekman thickness $h_E = \sqrt{2\nu/f}$, where $\nu$ is the oceanic turbulent viscosity or the molecular viscosity in the laboratory case. Given the crude nature of this approximation $h_E$ can be assumed fixed.

By introducing scales: shelf width $L_*$ for $x$, $y$; the depth at shelfbreak $H_*$ for fluid depth $H$; total shelf transport $Q$ for $\psi$; $\zeta_* = Q/(H_* L_*^2)$ for $\zeta$; fixed $f_*$ for the Coriolis parameter, and time scale $T_* = 1/f_*$ the equations are cast into nondimensional form appropriate for a numerical approach:

$$\zeta_t + J(\psi, \frac{f}{H}) + R_o J(\psi, \frac{\zeta}{H}) = -\frac{1}{2} R \frac{f}{H} \zeta, \tag{3}$$

with two small nondimensional parameters: Rossby number $R_o = \zeta_*/f_*$ and Rayleigh drag $R = h_E/H_*$. The elliptic equation remains the same.

In order to replicate the laboratory experiments and understand the dynamics better, we set up a simplified numerical model by rectifying the geometry and focusing on the NEC, see the rectangular domain and bathymetry in Fig. 11. The flow was driven by prescribing the kinematic boundary conditions on steam function $\psi$: the forced inflow with uniform velocity profile ($\psi(y)$ is specified), impermeability at the closed boundary segments ($\psi = 0$ offshore or $\psi = 1$ around the gulf and at the ridges), and the gradient outflow $\psi_x = 0$ (with the profile $\psi(y)$ developing as a part of the solution). These kinematic conditions are utilized in solving the elliptic equation. We note that specifying Dirichlet ($\psi = 0$) or Neumann condition ($\psi_y = 0$) at the abyssal ocean boundary has no effect on the solution because the flow there is vanishing and is established by the inflow conditions. This fact also justifies using a corresponding solid boundary in the laboratory experiment. The bathymetry was slightly smoothed over several grid steps at the shelfbreak in order to avoid discontinuities and spurious numerical artifacts. All derivatives then were replaced by standard centered differences. Without the lateral friction term a smooth solution of such a system generally asymptotes to a steady state. Furthermore, if one is interested only in the steady linear solution, then it is easy to reduce the problem to a banded sparse matrix formulation and solve it directly for fairly large grid sizes adequate for our purposes.

## 5 Numerical results

***Numerical Experiment***

In general, solutions of the above Eqs. 1 and 2 on a shelf are knows as shelf waves (Csanady 1978), which propagate along shore following geostrophic contours ($f/H$) with the shallower water on the right, in the northern hemisphere. These waves arise due to the topographic $\beta$-effect, sloping bottom, in a rotating fluid. Due to the dissipation in the bottom

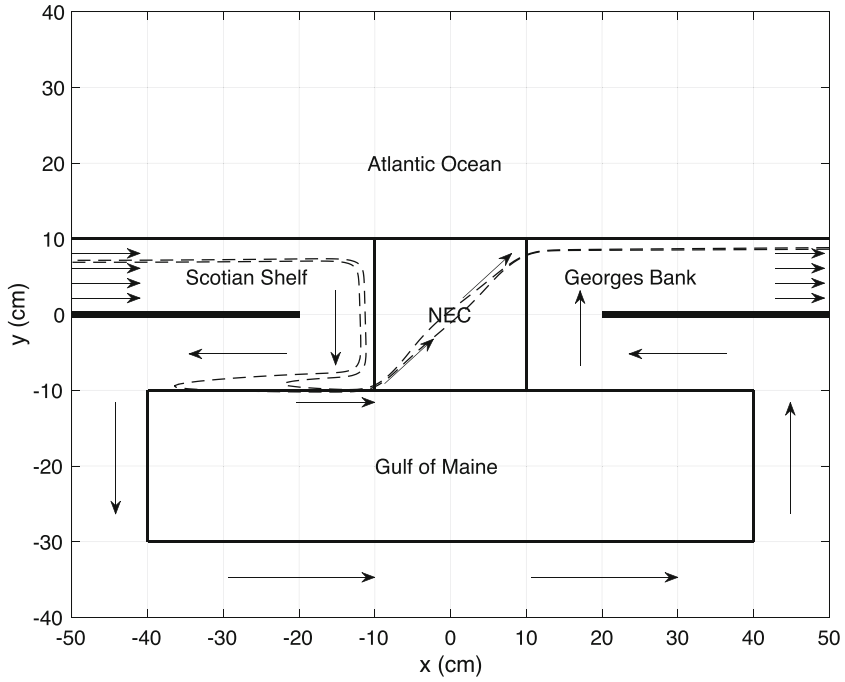


**Fig. 11** Computational domain. Georges Bank and Scotian Shelf are 2.5 cm deep, NEC is 4.5 cm deep, Gulf of Maine is 6.5 cm deep and the Atlantic is deepening from 16cm at the shelfbreak to 31cm towards the abyss. The horizontal dimensions are shown in cm in order to match with the sketch of the laboratory case. Indicated by dashed lines are two streamlines which represent the looping return flow required to match the flow transport on Georges Bank

Ekman layer, the time dependent transient solutions tend to decay exponentially with the time scale $T_B = 2H_*/(f_* h_E)$. From the analysis of low-frequency wind-driven motions, the decay time scale on the shelf can be estimated to be about 8 days (Chapman et al. 1988), which gives $R = h_E/H_* = 0.03$. The resulting steady solution is known as the arrested shelf wave or a topographic $\beta$-plume (for the steady, linear case see Kuehl (2014); for the steady, nonlinear case see 2018 and for the steady two-layer case see Kuehl and McMahon (2020); and with McMahon et al. (2020)). With the shelf running parallel to x, as in the inflow region, and a small aspect ratio ($\partial_x << \partial_y$) the dominant terms will be

$$\psi_x H_y = -\frac{1}{2} R H (\frac{1}{H}\psi_y)_y \tag{4}$$

This is analogous of the "heat equation" with $x$ being time and the second derivative $\psi_{yy}$ representing cross shelf diffusion.

An example of a linear numerical solution for small friction R=0.04 is shown in Fig. 12. One can clearly see the general flow along the shelf around the gulf. Some of the flow slowly leaks from the shelf into the gulf interior and then focuses into a jet crossing the strait diagonally, which is so conspicuous in the satellite images and our laboratory experiments.

In order to understand the formation of the peculiar flow diagonally crossing the strait, consider a steady slow flow, $R_o = 0$, without the bottom drag, $R = 0$; the stream lines

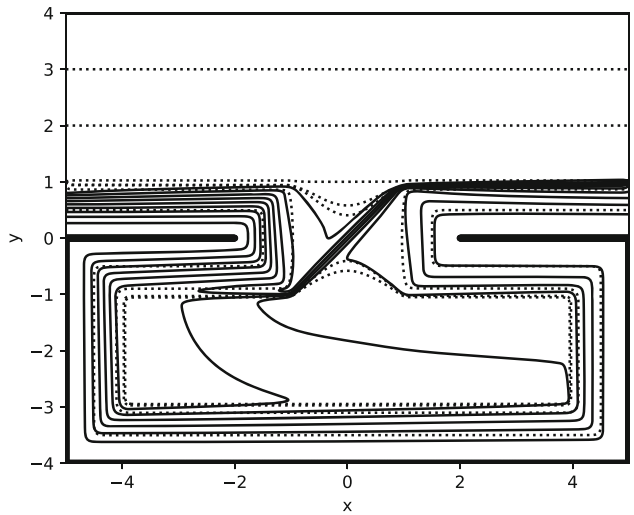


**Fig. 12** Numerical solution to Eqs. 2 and 3 with $R_o = 0$, $R = 0.04$. Dotted lines are the most representative isobaths. Slight smoothing of bathymetry in the numerical model results in appearance of a generic saddle point in the center of NEC. Solid lines are stream function with contour interval 0.1. Four streamlines crossing the NEC represent the crossover jet. The horizontal dimensions are scaled by the width of shelf

merely follow the geostrophic contours

$$J(\psi, \frac{f}{H}) = 0 \tag{5}$$

The typical Rossby number (nonlinearity) in this problem is rather small (see the table with parameters). Williams et al. (2001) showed that in order to negotiate a gap such as NEC due to the nonlinearity the currents must be non-realistically high, thus our choice of $R_o = 0$. If the inflow is restricted to the shelf, it will remain on the shelf while traveling around the gulf. Now consider the isobaths and streamlines near the shelfbreak. The slightly deeper isobaths (and corresponding streamlines) go directly to the Georges Bank shelf. The slightly shallower isobaths (and corresponding streamlines) take a much longer path (around the Gulf of Maine) and only then join the deeper lines. This causes no problem and the solution remains smooth and continuous because the stream function is preserved along the isobath.

This smooth and continuous reconnection is not robust when friction is present. With small friction, the flow will start to diffuse across isobaths as it flows along the shelf and tends to slowly move away from shore to deeper water. The streamlines following the deeper direct path to Georges Bank (leaping directly across the strait) experience negligible friction and remain at nearly the same depth. On the contrary, the streamlines that go around the gulf experience a much stronger frictional effect due to their much longer path, that is, the $\beta$-plume diffuses more and the streamlines spread into the middle of the gulf. Therefore, following the isobath along the longer path, the stream function on Georges Bank will have a different (somewhat larger) value where the isobaths reconnect and a jump in the stream function value will appear. Thus, a jet will form at the reconnection point of the isobaths arriving at the southern flank of Georges Bank. The source feeding this jet could not come from the northern part of the strait (Georges Bank side). That would imply that the jet went all around the gulf following the the geostrophic contour. The only possibility is to come diagonally across the strait from the area where the shelf flow enters the gulf. There, along the "shelfbreak" inside the gulf a return flow is formed which generates enough friction to close the discontinuity at the reconnection location. This return flow is shown schematically in Fig. 11. However, in Fig. 12 you can see the actual

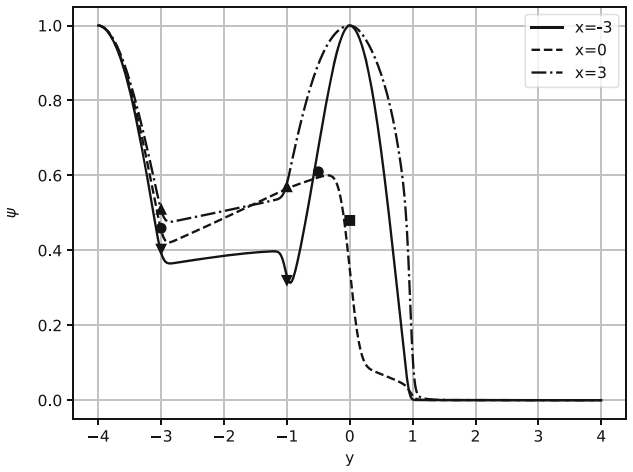


**Fig. 13** The sections of stream function $\psi(y)$ across the domain at $x = -3$ (solid), $x = 0$ (dashed), and $x = 3$ (dotdashed) for the bottom friction parameter $R = 0.04$. The comparison with the decay estimates based on the quasiparallel shelf flow theory (values of $\psi$ at the shelfbreak) are shown by downward triangles for $x = -3$, by circles for $x = 0$, by upward triangles for $x = 3$. The solid square mark at $y = 0$ shows the decay corresponding to the perimeter of the gulf shelfbreak of length 20

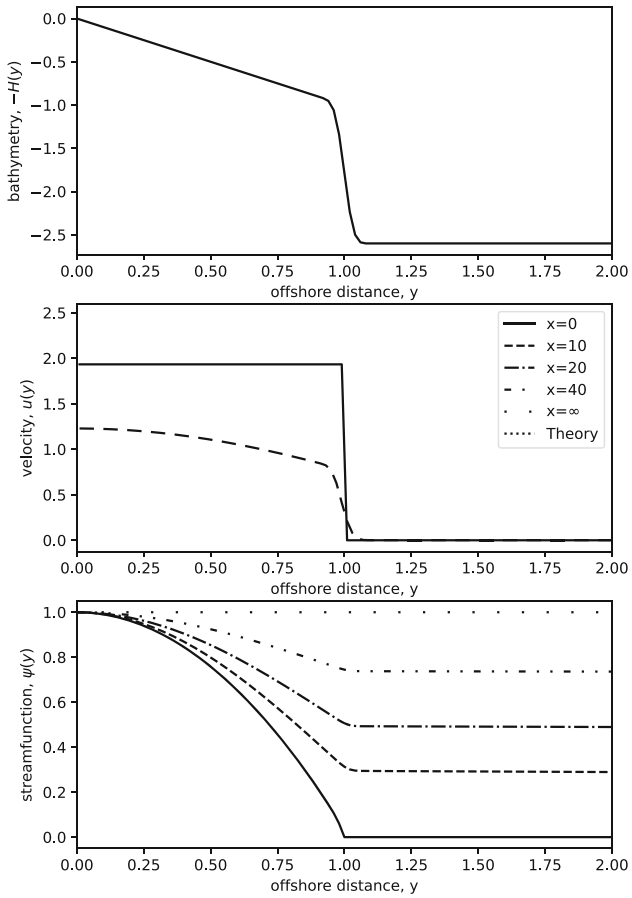


**Fig. 14** Numerical and theoretical solutions for a quasiparallel flow on a shelf. The top panel shows bathymetry as in the laboratory experiment (dotted line) with a jump at shelfbreak $H_2/H_1 = 2.6$; the solid line shows slightly smoothed bathymetry used in the numerical solution. The middle and bottom panels show velocity and stream function profiles across the shelf for several values $x$ in the numerical solution with $R = 0.04$. The solid line ($x = 0$) is the uniform inflow which decays downstream and quickly asymptotes to the theoretical profile shape shown by the dotted curve corresponding to the eigenvalue $k = 1.6334$. The numerical solution decay matches $\lambda = kR/2 = 0.032667$

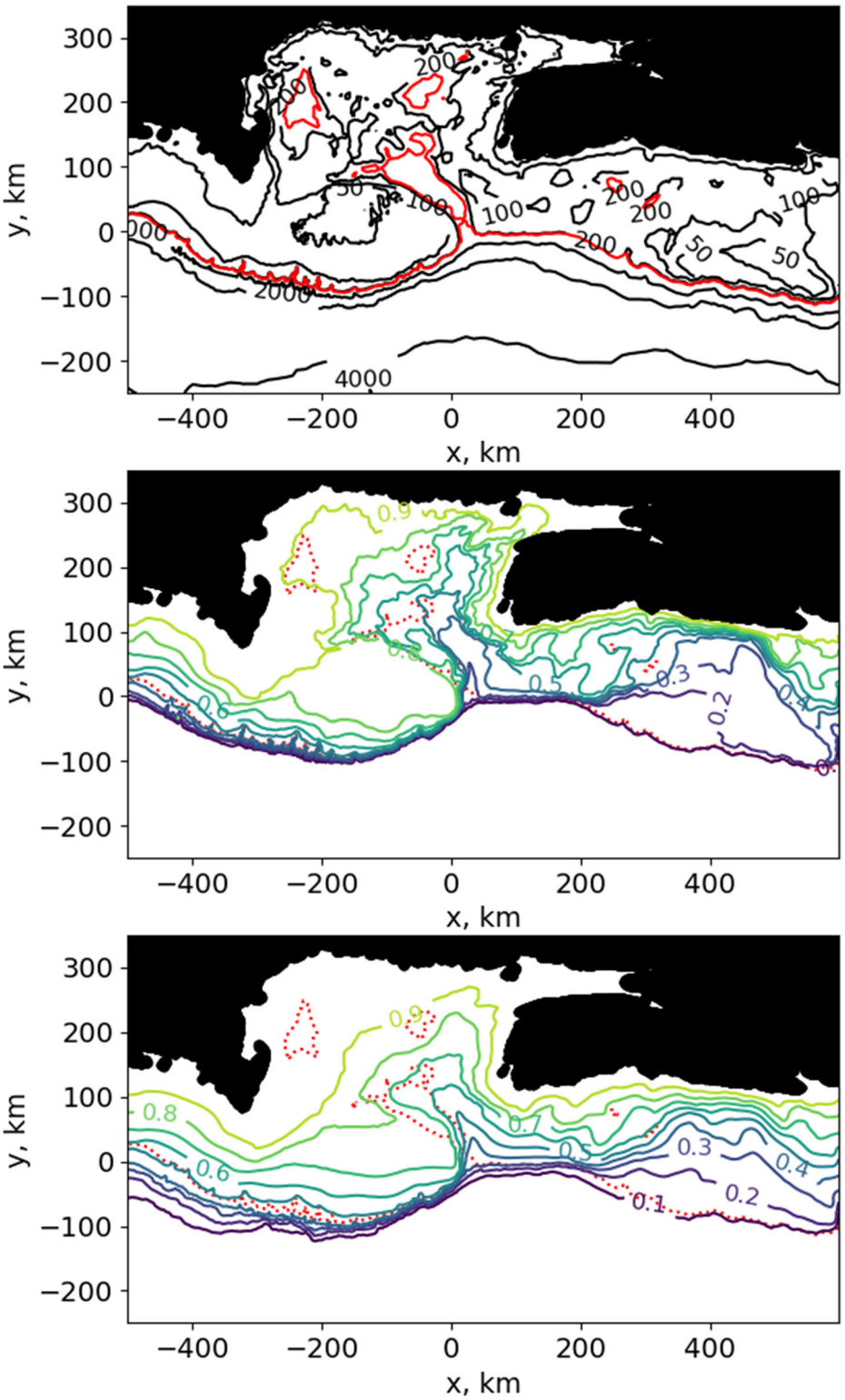


**Fig. 15** Numerical calculations for steady Gulf of Maine circulations at different values of bottom friction. Top panel shows Gulf of Maine bathymetry: 50, 100, 200, 1000, 2000, and 4000m isobaths in black. The red isobath corresponds to the NEC saddle point depth 234m. The stream function is plotted in Middle panel for $R = 0.04$ and in Bottom panel for $R = 0.2$. The colored solid isolines have a contour interval of 0.1 of the total transport. The dotted red line is the geostrophic contour $H/f$ passing through the saddle point and is very similar to the 234m isobath

streamlines making a tight loop and then diagonally crossing the strait.

The evolution of the flow is most clearly illustrated by the sections of the stream function $\psi(x, y)$ across the domain at three positions: $x = -3$, $x = 0$, and $x = 3$ (Fig. 13). For a small value $R = 0.04$, we see that a larger portion of the flow enters the gulf, $\psi(x = -3, y = -1) = 0.32$ (marked by downward triangle). As the flow circumnavigates the gulf the transport on the shelf diminishes due to friction: stream function values become larger, $\psi(x = 3, y = -1) = 0.58$ (marked by upward triangle). The jet crossing the strait is represented by a rapid drop of $\psi$ near $y = 0$ for $x = 0$ (dashed curve).

***Quasiparallel shelf flow***

In this section, when referring to the quasiparallel shelf flow, we assume that $y = 0$ is at the coast and $x$ is downstream (as in the Northern Gulf of Maine). In order to quantitatively describe the shelf flow along the perimeter of the Gulf of Maine, we consider a quasi-parallel flow on a shelf with a fixed profile $H(y)$ as in our laboratory case: the depth increases linearly with the distance offshore $y$ until the shelfbreak ($y = 1$) where a sudden jump in the bathymetry occurs from $H_1 = 1$ to $H_2$ and then remains constant as $y \to \infty$ (Fig. 14, top). The flow is driven by prescribing the inflow ($x = 0$) velocity $u = 2$ on the shelf and $u = 0$ in the deeper part (Fig. 14, middle, solid curve). The nondimentional velocity value is 2 because the area of a triangular shelf cross section is $\frac{1}{2}$ and the total flow is 1. Figure 14 depicts the evolution of the flow according to our numerical model for the simplified configuration in a linear case. One can see that the along shelf velocity profile $u(y)$ rapidly achieves an asymptotic shape with a roughly uniform value on the shelf and a jump at the shelfbreak. Both the velocity magnitude and the alongshelf transport decay downstream due to a slow leakage of the flow across the shelfbreak. A related problem of the shelf-slope flow leakage was considered in Hill (1995). The small offshore velocity $v$ is neglected in the frictional term due to the small aspect ratio ($\partial_x \ll \partial_y$).

Since this problem is uniform along the shelf the solution to the governing (4) can be sought using the separation of variables in the form $\psi(x, y) = 1 - \exp(-\lambda x)\phi(y)$, assuming that the flow decays exponentially with the distance $x$ along the shelf. We clarify that $\phi$ is the normalized structure function, while the alongshelf transports decays exponentially downstream. The streamfunction in the gulf interior is not fixed but varies along the shelfbreak due to the leakage of flow from the shelf.

The cross shelf structure function $\phi(y)$ satisfies a Sturm-Liouville problem with the eigenvalue $k = 2\lambda/R$

$$-H(\frac{1}{H}\phi_y)_y = kH_y\phi(y) \tag{6}$$

with the boundary condition of fixed stream function at the coast $\phi(0) = 0$ and $\phi(\infty) = 1$ representing the alongshelf transport.

Due to the discontinuity in the bathymetry at the shelf break, we have to consider two regions (shelf $0 < y < 1$ and the gulf interior $y > 1$) separately and use the jump condition

$$k \ln\left(\frac{H_2}{H_1}\right)\phi(1) = \left[\frac{\phi_y(1-0)}{H_1} - \frac{\phi_y(1+0)}{H_2}\right] \tag{7}$$

which is derived by integrating (6) across the shelfbreak. From the physical point of view we still assume the shallow water dynamical equations to be valid even at the shelfbreak. In order to find the numerical solution we slightly smoothed the discontinuity in the bathymetry. In the gulf interior $H_y = 0$ and the solution has to be $\phi(y) = 1$ everywhere, thus at the shelfbreak $\phi(1) = 1$. The right hand side of Eq. 7 represents the jump in the alongshelf velocity across the shelfbreak and the last term is vanishing.

On the shelf $H_y = 1$, with the linearly increasing depth $H = y$ the solution (6) can be expressed in terms of the Bessel functions

$$\phi(y) = C_1 y J_1(\sqrt{k}y) + C_2 y Y_1(\sqrt{k}y) \tag{8}$$

We note that the above substitution reduces (6) to the Bessel equation. Recall that for small arguments $J_1(z) \simeq z/2$ and $Y_1(z) \simeq -2/(\pi z)$. The coefficient $C_2$ must vanish in order to satisfy $\phi(0) = 0$ and $C_1 = 1/J_1(\sqrt{k})$ since $\phi(1) = 1$.

Thus in the eigenvalue problem for the shelf flow ($0 < y < 1$) the boundary conditions determine the coefficients $C_1$ and $C_2$ and the jump condition (6) determines the eigenvalue $k$ according to the implicit equation

$$k \ln(\frac{H_2}{H_1}) = \frac{\partial}{\partial y}(\frac{y J_1(\sqrt{k}y)}{J_1(\sqrt{k})}) = 1 + (\frac{\sqrt{k}J_1'(\sqrt{k})}{J_1(\sqrt{k})}) \tag{9}$$

where the derivative is evaluated at $y = 1$. There is an infinite set of $k$ satisfying (9) with corresponding flow structures $\phi(y)$, but we are interested only in the lowest mode with the smallest $k > 0$ that results in the slowest decay of the mode along the shelf $\lambda = kR/2$. The higher modes need to be considered if there are flow reversals at the inlet. Note that the lowest $k$ and the flow structure depend on the ratio of depths across the shelfbreak $H_2/H_1$. For $H_2/H_1 = 2.6$, as in the laboratory case, the lowest eigenvalue $k = 1.6334$. These theoretical solutions are shown in Fig. 14 by dotted curves. The predicted decay rate $\lambda = kR/2 = 0.032667$ matches that of the numerical solution.

For larger bathymetry jumps at the shelfbreak $k$ is getting smaller, e.g., $k = 0.7809$ for $H_2/H_1 = 10$, $k = 0.4115$ for

$H_2/H_1 = 100$. The velocity profile is more uniform over the shelf with a more pronounced discontinuity across the shelfbreak. Without the bathymetric jump $H_2 = H_1$, $k = 5.7830$ and the decay rate is substantially larger. The flow profile has no discontinuity in velocity and it vanishes at the edge of the shelf, $u(1) = 0$.

The alongshelf decay rate $\lambda$ obtained from solving the quasiparallel flow eigenvalue problem applies well to the interior of the gulf and to all segments of the shelf in Fig. 12, ignoring that the shelf makes 90 degree turns. We also resume using the $y$ coordinate to refer to points in Fig. 12. The triangle and circle marks in Fig. 13 indicate predictions of $\psi$ at the shelfbreak based on the formula $1 - \psi(-3, -1)\exp(-\lambda s)$, where $s$ is the distance along the shelfbreak inside the gulf from the first point $(x = -3, y = -1)$. With the total path length along shelfbreak in the gulf in our rectangular model $s = x/L = 20$, the decay, $a = \exp(-\lambda s) = 0.5203$ for $R = 0.04$, and $a = 0.03812$ for $R = 0.2$. In other words, $a$ represents the fraction of the transport that circumnavigates the gulf along the shelf. The corresponding estimate for the stream function values $\psi \simeq (1 - a)$ is marked by a solid square in Fig. 13 and agree well with the numerical solution. We note that the most dramatic changes in the flow pattern occur around the bottom drag parameter $R = 0.04$. Approximately half of the transport goes around the gulf and half crosses the strait diagonally, making the crossover jet most evident.

***Gulf of Maine***

Thus far, we have shown experimentally, numerically and justified theoretically that it is the splitting and reconnecting of isobaths for a linear, viscous flow that is the mechanism responsible for the peculiar diagonal flow pattern exhibited by shelf flows crossing over a strait. This work was motivated by observational data from the NEC of the Gulf of Maine. To further the relevance of this mechanism to more realistic ocean conditions, we apply our numerical model to the actual Gulf of Maine bathymetry. Figure 15 (top panel) illustrated the bathymetry and domain considered. The middle and lower panels represent calculations for $R = 0.04$ and $R = 0.2$, respectively. Note that the highlighted red isobath of 234m in the top panel and the geostrophic contour in the middle and lower panels (shown with a dotted red line) are passing through the NEC saddle point. It is immediately obvious that for realistic values of bottom drag ($R \approx 0.04$), the Gulf of Maine system admits the peculiar, diagonal flow pattern similar to that observed in our laboratory and numerical experiments, as well as was suggested by observational data. Note how many isolines penetrate deep into the Northern Gulf of Maine, return and then cross the NEC. As expected, when the bottom drag is increased, a more broad, diffuse flow is observed crossing the NEC, consistent with our findings described above. The dependence of the cross-strait flow pattern on bottom drag parameterization should be noted as it implies the importance of bottom drag parameterizations for accurate modeling of large-scale flow patterns.

We noted in the introduction that the crossover events are most dramatic in spring, when the stratification is weaker, and the bathymetric steering is therefore more important. This is consistent with our finding that the geostrophic contour splitting combined with the right amount of bottom drag can cause dramatic diagonal flows.

## 6 Conclusion

Thus, the peculiar jet crossing the strait diagonally is a robust feature which is formed due to the splitting of the flow into short and long pathways (correspondingly with less and more friction). Upon reconnect of these two pathways, a jet is formed due to the discontinuity in stream function caused by differential accumulation of frictional modification, and the source of the jet is a frictional return flow. Ultimately, we have proven the existence of such peculiar, diagonal crossover flow states and uncovered their fundamental governing dynamics. We have also shown that such flow patterns do indeed exist as solutions to Eqs. 2 and 3 for the actual Gulf of Maine bathymetry. It is yet to be shown that these same dynamics are robust to the stratified, time dependent Gulf of Maine circulation, but the fundamental nature of our findings to generic oceanographic systems, such as the Gulf of Maine, provide powerful motivation for their existence. Additionally, the stability characteristics of this peculiar state remain an interesting open question.

**Acknowledgements** The work was launched with the support from the National Science Foundation Grant OCE-0351518. Continuing efforts to the fruition of this work have been with support from the National Science Foundation Grant number 1823452 and the Texas General Land Office Grant number 18-130-000-A670. The initial experiments were conducted on a 1m turntable at the Geophysical Fluid Dynamics Laboratory of the Graduate School of Oceanography, University of Rhode Island. The later experiments were conducted on a 2m turn table at the Geophysical Fluid Dynamics Laboratory at Woods Hole Oceanographic Institution.

**Availability of data and materials** The data used in this manuscript is publicly available and the numerical codes are available at the corresponding author's website (http://sites.udel.edu/kuehl-group/software/) or upon reasonable request to the corresponding author.

## Declarations

**Conflict of interest** The authors declared that they have no conflict of interest.

## References

Beardsley RC, Butman B, Geyer WR, Smith PC (1997) Physical oceanography of thegulf of maine: an update. Gulf of Maine Ecosystem Dynamics: a Scientific Symposium and Workshop, RARGOM Report 97–1:39–52

Bisagni JJ, Smith PC (1998) Eddy-induced flow of scotian shelf water across Northeast Channel, Gulf of Maine. Continental Shelf Res 18:515–539

Bisagni JJ, Beardsley RC, Rusham CM, Manning JP, Williams W (1996) Climatological effects of toporography and land-sea heating contrasts on the gravity wave-driven circulation of the mesosphere. Deep-Sea Res 43:1439–1471. https://doi.org/10.1175/1520-0469(2003)060<0103:CEOOAL>2.0.CO;2

Chapman DC (2003) Separation of an advectively trapped buoyancy current at a bathymetric bend. J Phys Oceanography 33:1108–1121

Chapman DC, Lentz SJ, Brink KH (1988) A comparison of empirical and dynamical hindcasts of low-frequency, wind-driven motions over a continental shelf. J Geophys Res 93(C10):12409–12422

Cho YK, Beardsley RC, Sheremet VA (2002) On the cause of Scotian Shelf Crossovers. Geophys Res Lett 29(24):2212. https://doi.org/10.1029/2002GL014968

Csanady GT (1978) The arrested topographic wave. J Phys Oceanography 8:47–62

Garret C (1995) Flow separation in the ocean. In: Topographic effects in the ocean. Proceedings 'Aha Huliko'a Hawaiian Winter Workshop, University of Hawaii at Manoa, 119–124

Gill AE (1982) Atmosphere-Ocean Dynamics. Academic Press

Hill AE (1995) Leakage of barotropic slope currents onto the continental shelf. J Phys Oceanography 25(7):1617–1621

Ibanez R, Kuehl J, Shrestha K, Anderson W (2018) A nonlinear self-similar solution to barotropic flow over rapidly varying topography. Nonlinear Process Geophys 25:201–205

Klinger B (1994) Inviscid current separation from rounded capes. J Phys Oceanography 24:1805–1811

Kuehl JJ (2014) An analytic solution for barotropic flow along a variable slope topography. Geophys Res Lett 41. https://doi.org/10.1002/2014GL061188

Kuehl J, McMahon C (2020) An analytic solution for bottom intensified flow along sloping topography. European J Mech B: Fluids 82:156–160

Kuehl J, Sheremet VA (2009) Identification of cusp catastrophe in gap leaping western boundary current problem. J Marine Res 37(1):25–42

Kuehl JJ, Sheremet VA (2014) Two-layer gap-leaping oceanic boundary currents: experimental investigation. J Fluid Mech 740:97–113

Lee C, Brink K (2000) 26 june - 6 july, 1997 en303, R/V Endeavor, Seasoar observations of loss and retention processes over the southern flank of Georges Bank. Slope Water Interaction Workshop

Limeburner R (2019) Drifter track data from drifters deployed on multiple R/V Endeavor, Albatross IV, Oceanus, Delaware, Cape Hatteras, Parizeau, and Ccgs Cygnus Cruises in the Gulf of Maine and Georges Bank from 1995–1999 (globec). Technical report, WHOI. https://doi.org/10.1575/1912/bco-dmo.3660.1. https://hdl.handle.net/1912/23627

Manning JP, McGillicuddy Jr. DJ, Pettigrew NR, Churchill JH, Incze LS (2009) Drifter observations of the gulf of maine coastal current. Continental Shelf Res) 29(7):835–845

Manning JP, Beardsley RC (1996) Assessment of georges bank recirculation from eulerian current observations in the great south channel. Deep-Sea Research II (GLOBEC Special Issue) 43(7–8):1575–1600

McMahon CW, Kuehl JJ, Sheremet VA (2020) A viscous, two-layer western boundary current structure function. Fluids 5(2):63

Mountain DG, Manning JP (1994) Seasonal and interannual variability in the properties of the surface waters of the gulf of maine. Continental Shelf Res 14(13–14):1555–1581

Sheremet VA (2001) Hysteresis of a western boundary current leaping across a gap. J Phys Oceanography 31:1247–1259

Sheremet VA, Kuehl J (2007) Gap leaping western boundary current in a circular tank model. J Phys Oceanography 37:1488–1495

Sheremet VA, Khan AA, Kuehl J (2022) Multiple equilibrium states of the gulf of Mexico loop current. Ocean Dynamics 72:731–740

Smith PC (1983b) Eddies and coastal interactions. Eddies in Marine Sci –20446480

Smith PC (1989) Seasonal and interannual variability off southwest nova scotia. Canadian J Fisheries Aquatic Sci 45 (supp. 1:4–20ss

Smith PC, Houghton RW, Fairbanks RG, Mountain DG (1997) Interannual variability of boundary fluxes and water mass properties in the gulf of maine and on georges bank: 1993-97. ices c.m. ICES Annual Science Conference 32

Smith PC (1983) The mean and seasonal circulation off southwest nova scotia. J Phys Oceanography 13:1034–1054

Smith PC, Flagg CN, Limeburner R, Fuentes-Yaco C, Hannah C, Beardsley RC, Irish J (2003) Scotian shelf crossovers during winter/spring 1999. J Geophys Res 108:8013. https://doi.org/10.1029/2001JC001288

Williams JW, Gawarkiewicz GG, Beardsley RC (2001) The adjustment of shelfbreak jet to cross-shelf topography. Deep-Sea Research Part II 48:373–393

Wishner KF, Gifford DJ, Sullivan BK, Bisagni JJ, Outram DM, Keuren DEV (2003) Biological signature of scotian shelf water crossovers on georges bank during spring 1997. J Geophys Res 108(C11):10–10292001001266

Wolfe CL, Cenedese C (2006) Laboratory experiments on eddy generation by a buoyant coastal current flowing over variable bathymetry. J Phys Oceanography 36:395–411